:PAGEversion9R;

K2 Compuscript [compuscript] - fot236 /data/journal/bioc bioc.b bioc2538.k root Thu Feb 11 12:32:54 1999 full terminal narrow nolist laser paper newhyph port cols:1 /data/K2/bin/seta ul:3000 priority:10

ELSEVIER

Biophysical Chemistry 76 (1999) 145–159

Biophysical Chemistry

Peptide–bilayer interactions: simulations of dermaseptin B, an antimicrobial peptide

P. La Rocca[a], Y. Shai[b], M.S.P. Sansom[a,*]

[a] *Laboratory of Molecular Biophysics, The Rex Richards Building, Department of Biochemistry, University of Oxford, South Parks Road, Oxford, OX1 3QU, UK*

[b] *Department of Membrane Research and Biophysics, Weizmann Institute of Science, Rehovot 76100, Israel*

Received 1 September 1998; received in revised form 9 December 1998; accepted 9 December 1998

Abstract

Dermaseptins, a family of antimicrobial peptides, are believed to act by forming amphipathic α-helices which associate with the cell membrane, leading to its permeabilisation and disruption. A simple mean field method is described for simulation of the interactions of peptides with lipid bilayers which includes an approximate representation of the electrostatic effects of the head-group region of the bilayer. Starting from an atomistic model of a PC phospholipid bilayer we calculate an average electrostatic potential along the bilayer normal. By combining the interaction of the peptide with this electrostatic potential and with the hydrophobic core of the membrane we arrive at a more complete description of peptide–bilayer energetics than would be obtained using sidechain hydrophobicities alone. Using this interaction potential in MD simulations of the frog skin peptide dermaseptin B reveals that the lipid bilayer stabilises the α-helical conformation of the peptide. This is in agreement with FTIR data. A surface associated orientation thus appears to be the most stable arrangement of the peptide, at least at zero ionic strength and without taking acccount of possible peptide–peptide interactions.

Keywords: Peptide; Bilayer; Antimicrobial; Dipole potential; α-helix; Molecular dynamics

1. Introduction

A number of antimicrobial peptides are believed to act by forming amphipathic α-helices which by associating with cell membranes, lead to subsequent membrane disruption and permeabilisation [1,2]. These peptides may be classified as membrane-perturbing, to distinguish them from channel-forming peptides [3]. Molecular characterisation of the interactions of such peptides with lipid bilayers is thus a key step towards understanding their mode(s) of action. Furthermore, the nature of the interactions with bilayers of such relatively simple peptides may provide

* Corresponding author. Tel.: +44 1865 275371, fax: +44 1865 275182, e-mail: mark@biop.ox.ac.uk

0301-4622/99/$ - see front matter
PII: S0301-4622(98)00232-4

clues as to possible folding mechanisms for membrane proteins in general.

The dermaseptins, isolated from frog skin, are a family of membrane-perturbing peptides [4–8]. They are 27–34 residues in length and inhibit the growth of bacteria, protozoa and fungi. They adopt a largely α-helical conformation when in a membrane-mimetic environment and bind to phospholipid bilayers. Synthetic dermaseptin B (DS-B) has been shown to bind tightly to both zwitterionic and negatively charged phospholipid vesicles in a non-cooperative manner [9], supporting a surface location rather than formation of an oligomeric bundle of bilayer-inserted helices. Modelling the sequence of this 31-residue peptide as an idealised α-helix reveals it to be highly amphipathic (Fig. 1). It is thus of interest to investigate in more detail the nature of the interaction of DS-B with lipid bilayers. In particular, one would like to be able to predict whether DS-B (and related peptides) prefers to associate with the surface of a bilayer (as do some other basic antimicrobial peptides e.g. cecropin P1; [10], or whether it inserts into lipid bilayers to form a transmembrane helix (as do number of channel forming peptides; [3,11]).

In order to study peptide–bilayer interactions, one may adopt a simulation approach in which the bilayer is mimicked by an empirical energy function. In one such approach the bilayer is treated as a simple continuum hydrophobic slab, with only the peptide being modelled in atomic detail [12–16]. Such models have been employed successfully in studying e.g. voltage-induced insertion of channel-forming peptides [17]. However, the approximation of the bilayer as a hydrophobic slab is somewhat simplistic. Joint X-ray and neutron diffraction studies [18] have shown that lipid bilayers have a wide (approx. 10–15 Å) interfacial region between the bulk aqueous solvent and the

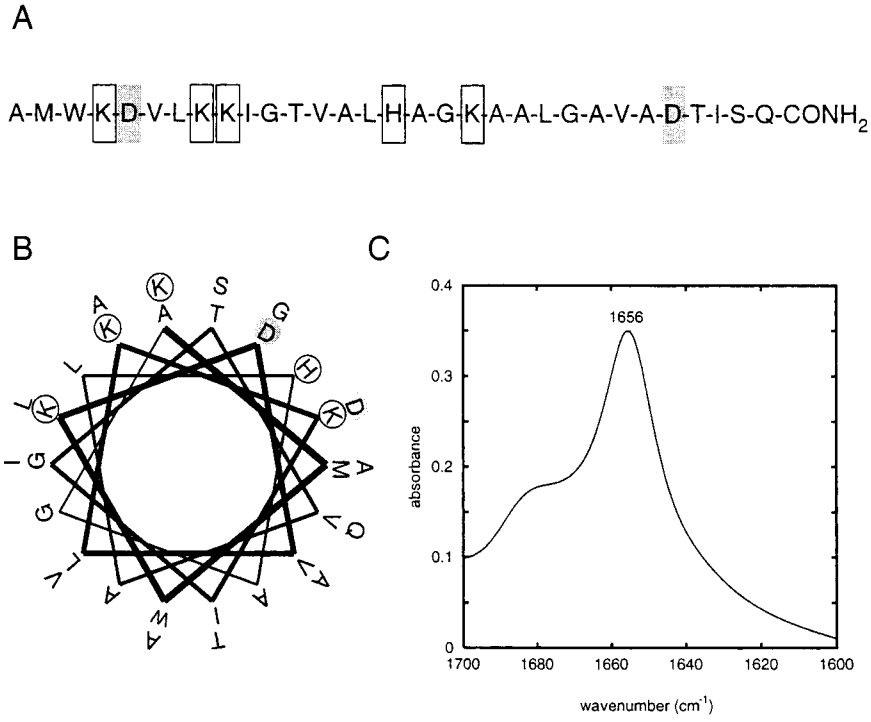

Fig. 1. (A) Sequence of dermaseptin B (DS – B). Basic residues are indicated by an empty box, acidic residues by a grey box. (B) Helical wheel projection of the DS-B sequence. Basic residues are indicated by an empty circle, acidic residues by a grey circle. (C) FTIR spectrum for DS-B in a phospholipid bilayer. The pronounced peak at 1656 cm^{-1} is indicative of a high α-helical content.

hydrophobic core of the membrane. In this region the polar head groups of the phospholipids coexist with water molecules. This view is reinforced by a number of molecular dynamics (MD) simulations of pure lipid bilayers [19–24]. Furthermore, a number of experimental studies on the differential permeability of lipid bilayers to anions and cations across membranes suggest that the orientated molecular dipoles within the interface generates a dipole potential in this region [25,26]. Such an interfacial dipole potential will have a profound effect on the energetics of interaction of charged amphipathic peptides with lipid bilayers. Thus, whilst it is desirable to retain the simplicity of an empirical bilayer potential in simulations of peptide–bilayer interactions, it is important that the interfacial dipole potential is taken into account. In this paper we employ an atomistic model of a phosphatidylcholine bilayer generated in large scale MD simulations by Schulten et al. [19] to derive an approximate interfacial electrostatic-term which is included in an empirical bilayer potential within the MD simulation program CHARMm [27]. This potential is then used to investigate the interaction of DS-B with a zwitterionic bilayer, and the simulation results compared with experimental data on DS-B conformation in the presence of a phospholipid bilayer. A preliminary account of some of these studies has appeared in abstract form [28].

2. Methods

2.1. Experimental

2.1.1. Peptide synthesis

Synthesis and purification of DS-B was as described [9]. Briefly, *t*-Boc chemistry was used to synthesize the peptide on PAM resin. The peptide was purified by reverse-phase HPLC.

2.1.2. ATR-FTIR measurements

Spectra were obtained using a Perkin-Elmer 1600 FTIR spectrometer coupled with an ATR device. For each spectrum, 512–1024 scans were collected, with resolution of 2 or 4 cm^{-1}. Samples were prepared as previously described [10]; briefly, a mixture of PE/PG (1 mg) alone or with peptide (130 μg) was deposited on a Germanium prism ($52 \times 20 \times 2$ mm). The aperture angle of 45° yielded 25 internal reflections. Lipid–peptide mixtures were prepared by dissolving them together in a 1:2 methanol/CH_2Cl_2 mixture and drying under a stream of nitrogen. Spectra were recorded either with dry samples or wet with D_2O and the respective pure phospholipid was subtracted to yield the difference spectra. The background was a clean Germanium prism.

2.2. Theoretical and computational

2.2.1. Interfacial electrostatic potential of a lipid bilayer

A model of a POPC bilayer (200 lipid molecules and 5483 water molecules) in the fluid phase from the MD simulation of [19] was downloaded from http://www.umass.edu/microbio/rasmol/bilayers.html. This coordinate set was used as the basis of calculation of the approximate electrostatic potential along the bilayer normal (*z*-axis). Calculations of the potential based on an independent PC bilayer MD [20] yielded similar results.

The electrostatic potential along the bilayer normal may be obtained by solution of the Poisson equation:

$$\nabla\varepsilon(\mathbf{r})\nabla\Phi(\mathbf{r}) = -\frac{\rho(\mathbf{r})}{\varepsilon_0} \quad (1)$$

where $\Phi(\mathbf{r})$, $\varepsilon(\mathbf{r})$ and $\varepsilon(\mathbf{r})$ are the electrostatic potential, dielectric constant and charge density, respectively at position $\mathbf{r}$. In our calculations we treated the phospholipid atomistically, deriving the charge density $\rho(\mathbf{r})$ from the coordinates and atomic partial charges of the POPC molecules (Fig. 2). Water was treated as a *z*-dependent dielectric constant. Although this is a simplification (see Discussion) it captures the essence of the electrostatic potential along the bilayer normal at a similar level of approximation to the other elements of the empirical energy function used to represent the bilayer. At any single point in time the electrostatic potential from solution of Eq. (1) will depend on *x*, *y*, and *z* (where the *xy* plane is that of the membrane). However, on

the timescale of peptide–bilayer interactions the peptide is assumed to experience a potential which is averaged in the membrane plane:

$$\overline{\Phi}(z) = \frac{1}{S}\int \Phi(\mathbf{r})\mathrm{d}x\,\mathrm{d}y \tag{2}$$

where the integral in Eq. (2) is extended on a surface of the xy plane over an area S, sufficient to contain 100 lipid molecules. In the case of a dielectric function dependent on z, the average potential $\overline{\Phi}(z)$ is the solution of Eq. (1) with an average charge distribution on the right hand side of the equation:

$$\varepsilon(z)\frac{\mathrm{d}^2\overline{\Phi}(z)}{\mathrm{d}z^2} + \frac{\mathrm{d}\varepsilon}{\mathrm{d}z}\frac{\overline{\Phi}(z)}{\mathrm{d}z} = -\frac{\overline{\rho}(z)}{\varepsilon_0} \tag{3}$$

where

$$\overline{\rho}(z) = \frac{1}{S}\int \rho(\mathbf{r})\mathrm{d}x\,\mathrm{d}y \tag{4}$$

and where the definition of integral and S are the same as in Eq. (2). To construct an average charge distribution the mean and standard deviation of the z coordinate of each of the phospholipid atom types were calculated. The contribution to the overall charge density of the bilayer from a particular atom type was approximated as a Gaussian function with mean and standard deviation as just calculated, and normalised to the partial charge per unit area of that atom type:

$$\overline{\rho}(z) = \frac{1}{A}\sum_i q_i G_i(z) \tag{5}$$

where A is the area per head group [19], q_i is the partial charge of atom type i (see Fig. 2), G is a Gaussian function of the z coordinate for atom type i, and where the sum is extended over all atom types of the phospholipid molecule. Note that the average of z across both leaflets of the bilayer is taken. Thus the resultant charge density of the bilayer is symmetrical about the centre of the bilayer ($z = 0$ Å). The charge density profile (Fig. 3A) has a maximum at z approx. ± 22 Å corresponding to the choline group and a minimum at z approx. ± 17 Å corresponding to the phosphate group. The model of the dielectric profile along the bilayer normal, $\varepsilon(z)$, used by Flewelling and Hubbel [25] was adopted:

$$\varepsilon(z) = \varepsilon_1 + (\varepsilon_2 - \varepsilon_1)[1 + 10^{4(d-z)/h}]^{-1} \quad \text{for } z > 0 \tag{6}$$

where $\varepsilon_1 = 2$ is the value of the dielectric constant in the hydrophobic core of the membrane, and where $\varepsilon_2 = 78$ is the value of the dielectric constant in bulk water. This function provides a smooth transition between the two dielectrics in the interfacial region (Fig. 3B), defined by two parameters d and h, respectively equal to the centre and width of the transition region. The extent of the bilayer is $z = \pm(d + h/2)$. Eq. (3) was solved using a finite difference algorithm [29]. A boundary condition of zero potential at $z = \pm 50$ Å (relative to the centre of the bilayer at $z = 0$) was imposed.

The calculation of the electrostatic potential along the bilayer normal was repeated for different values of the two parameters d and h. From Fig. 3C it is evident that the shape of the potential in the middle of the bilayer is sensitive to the value of d. In contrast, calculations for different values of h revealed that this parameter influences the potential to a lesser extent. Values of d and h were chosen to match (albeit approximately) the concentration of water molecules along the bilayer normal. One of the main char-

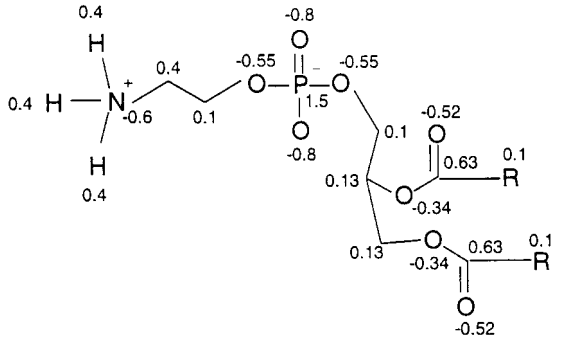

Fig. 2. Diagram of a phosphatidylcholine molecule indicating the partial charges employed in the headgroup potential calculations.

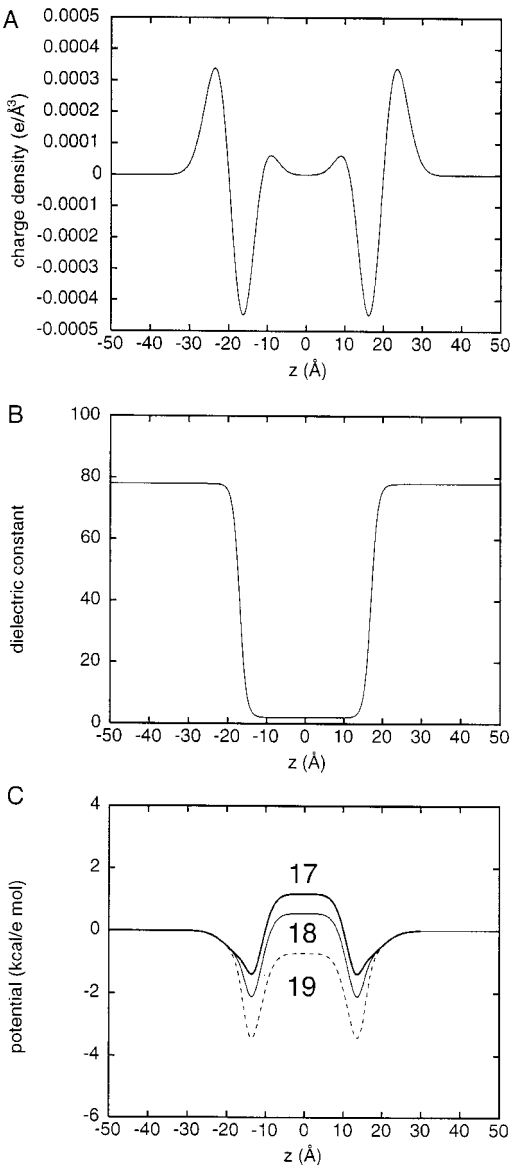

Fig. 3. (A) Charge density profile along the bilayer perpendicular (z). (B) Dielectric constant profile. (C) Electrostatic potential profiles, for $d = 17$ Å (bold line), 18 Å (thin line) and 20 Å (dashed line). Note that $d = 17$ Å was used in all subsequent simulations.

acteristics of the calculated average potential is a pronounced well, whose position ($z \sim \pm 14$ Å) is independent of the value of d adopted. Experimental estimates of the value of the difference in electrostatic potential between the aqueous phase adjacent to the bilayer and the centre of the bilayer (the 'dipole potential') [25,30–32] agree on a potential positive in the bilayer interior, although the estimated values extend over a rather broad range (+100 to +500 mV). In our calculations values of $d = 17$ Å and $h = 8$ Å yield a potential positive in the middle of the membrane and have been used throughout subsequent simulations. These values are compatible with the distribution of water molecules along z in the MD simulation used as the basis of our calculation [19].

2.2.2. Potential energy function for peptide–bilayer interactions

Energy calculations and MD simulations of peptide–bilayer interactions employed the CHARMm V23.3 potential energy function [27] and PARAM19 parameter set to evaluate the internal energy of the peptide, supplemented by an empirical term representing peptide–bilayer interactions:

$$E = E_{\mathrm{CHARMM}} + E_{\mathrm{CORE}} + E_{\mathrm{HEADGROUP}}. \quad (7)$$

E_{CHARMM} is the standard CHARMm potential, E_{CORE} is the hydrophobic interaction energy of the peptide with the bilayer core and $E_{\mathrm{HEADGROUP}}$ is the approximate electrostatic interaction energy of the peptide with the potential due to the lipid head groups as calculated above.

The hydrophobic interaction was calculated in a manner based on that of Edholm and Jähnig [33], as in our previous studies of peptide–bilayer interactions [15,17]:

$$E_{\mathrm{CORE}} = \sum_i h_i f(z_i) \quad (8)$$

where h_i is a hydrophobicity potential for sidechain i (based on the scale of Milik and Skolnick [13] for residues in an α-helical conformation), where the sum is extended to all the residues of the peptide and

$$f(z) = \frac{1}{2}\exp[-(|z| - d)/\lambda] \quad \text{for } z \geq d$$

$$f(z) = \frac{1}{2}\{2 - \exp[-(|z| - d)/\lambda]\} \quad \text{for } z \leq d \quad (9)$$

This functional form for $f(z)$ implies that $f(z)=0$ for $|z| \gg d$ and $f(z)=1$ for $|z| \ll d$, where d defines the transition from 'bulk' to 'bilayer' as defined above. The value of λ is 1 Å.

The electrostatic term representing the effects of the head groups is given by:

$$E_{\mathrm{HEADGROUP}} = c \sum_i q_i \overline{\Phi}(z_i) \quad (10)$$

where the sum is extended to all the atoms of the peptide and q_i and z_i are, respectively the partial charge and the z coordinate of the atom i of the peptide and where $\overline{\Phi}(z)$ is the electrostatic potential profile along the bilayer normal as calculated above. The constant c is introduced to scale the headgroup potential to the corresponding experimental estimate of the dipole potential. A value of $c=2$ was used throughout this study, corresponding to a dipole potential (measured from $z=-13.6$ Å to $z=0$ Å) of approx. $+220$ mV, which is similar to that described by e.g. Cafiso [26].

2.2.3. Models of peptides

Experimental studies have indicated that dermaseptins adopt a largely α-helical conformation when in a hydrophobic environment [4,6,7] or in the presence of a phospholipid bilayer (see Results). An ensemble of α-helical models of DS-B was generated by restrained molecular dynamics, as described previously [34] using X-plor v3.1 [35]. A structure from this ensemble was selected as being the closest to the ensemble average structure, and was subsequently used as the starting point for simulations.

2.2.4. MD simulations

MD simulations were performed using CHARMm v23.3 [27]. In all simulations an extended atom representation was used, with only those H atoms bonded to non-carbon atoms (polar hydrogens) treated explicitly. MD simulations consisted of a heating stage from 0 K to 300 K of 6 ps, and an equilibration and production stage during which velocity rescaling was applied in order to maintain the temperature within a window of 290–310 K. A time step of 0.5 fs was used. Distance restraints between backbone H and O atoms were *not* applied, in order to allow local deviations from α-helical geometry during the course of the simulations. For intramolecular electrostatic interactions, unless stated otherwise, a distance dependent dielectric ($\varepsilon = r$) was used in conjunction with a switching function and a cutoff distance of 9 Å, in order to mimic solvent screening of e.g. sidechain–sidechain interactions.

2.2.5. Analysis of trajectories

Display of structures and trajectories was performed using Quanta v4.0 (Molecular Simulations). Structure diagrams were drawn with Molscript [36]. All auxiliary programmes were written in Fortran 77. Secondary structure analysis was based on definition of the regions of the Ramachandran plot in Procheck [37].

3. Results

3.1. Peptide conformation

Before modelling DS-B–bilayer interactions it is important to confirm that is reasonable to assume that DS-B adopts a largely α-helical structure is such an environment. So, FTIR spectroscopy was used to determine the structure of DS-B in dry or wet PE/PG (7:3) membranes at a peptide:lipid ratio of 1:40. The amide I region between 1648 and 1660 cm^{-1} is characteristic of α-helical structure [38]. Deconvolution of the amide I region was performed using PEAKFIT and the result for DS-B is shown in Fig. 1C. The peptide was found to adopt 75% α-helix structure in either dry or wet phospholipid membranes. In aqueous solution the CD spectrum (data not shown) of DS-B suggested a completely random coil conformation. Thus, in simulations of DS-B–bilayer interactions, the starting structure for the peptide was an α-helix.

3.2. The energetics of DS-B–bilayer interactions

Before discussing the results of MD simulations, insights into the energetics of the interactions of DS-B with a PC bilayer may be obtained

by exploring the peptide–bilayer interaction energy (i.e. $E_{CORE} + E_{HEADGROUP}$) as a function of the position and orientation of a (rigid) DS-B helix. Such information also helps in choosing a low energy configuration of the system as a starting point for MD simulations. The change in the potential energy of a peptide held in a rigid α-helical conformation whilst translocated across the lipid bilayer is analysed. In order to explore the energetics of such interactions it is first necessary to define a coordinate system for the peptide helix (Fig. 4). As the bilayer potential depends only on z, a helix orientation can be defined in terms of the z coordinate of its centre relative to the centre of the bilayer ($z = 0$), and two angles. For a highly amphipathic helix, such as that of DS-B at the bilayer surface, rotation about its long axis through an angle θ results in either its hydrophilic face ($\theta = 0°$) or its hydrophobic face ($\theta = 180°$) being directed towards the water (Fig. 4A). Similarly, a helix located at the bilayer surface may be inserted into the bilayer by rotation about an axis perpendicular to its long axis from an angle of $\varphi = 90°$ (a surface associated orientation, perpendicular to the bilayer normal) to either $\varphi = 0°$ (C-terminal insertion) or $\varphi = 180°$ (N-terminal insertion), assuming $z \gg 0$ Å.

A simple first calculation of the energetics of DS-B–bilayer interactions compares inserting the helix into the bilayer with the long axis either perpendicular ($\varphi = 90°$; Fig. 5A) or parallel ($\varphi = 180°$; Fig. 5B) to the bilayer normal. Helices were then translated relative to the bilayer keeping φ fixed. Note that for $\varphi = 90°$ calculation, the helix was set to $\theta = 0°$ such that its hydrophilic face was directed towards the bulk water for positive z values. The two components of the interaction energy may then be displayed as functions of z. It is evident that for this charged peptide the contributions of E_{CORE} and of $E_{HEADGROUP}$ are of comparable magnitude. Thus neither term dominates the peptide–bilayer interaction energy to the exclusion of the other. However, it should be noted that $E_{HEADGROUP}$ was calculated for zero ionic strength, and at higher (physiological) ionic concentrations the strength of such interactions may be decreased. In the case of insertion with the DS-B helix parallel to the bilayer surface (Fig. 5A), the potential energy profiles have a relatively simple shape as a result of the amphipathic nature of the helix. There is a clear minimum interaction energy configuration with the helix at z approximately +17 Å, i.e. at the bilayer surface with its hydrophilic residues directed away from the bilayer core. A simple interpretation of the results for the insertion of the helix when oriented perpendicular to the bilayer surface (Fig. 5B) was not possible. However, again an energy minimum occurs (relative to the configuration with the helix fully removed from the bilayer). This suggested that a more systematic exploration of the energy surface of DS-B–bilayer interactions should be performed.

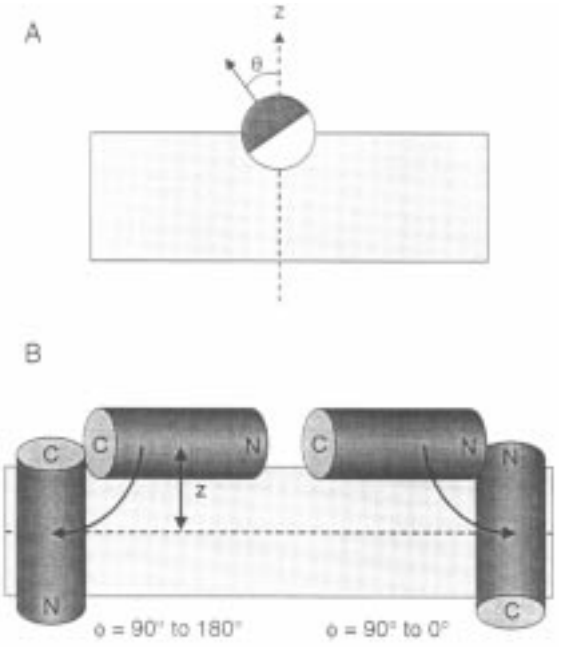

Fig. 4. Definition of the coordinate systems used. (A) An amphipathic helix, viewed end on, at the surface of a bilayer (shaded area). The dark grey segment of the circle represents the hydrophilic face of the helix. Thus, a rotation angle, θ, about the helix long axis relative to the bilayer normal is defined. (B) Definition of the two coordinates (z and φ) used in calculations of peptide–bilayer interaction energy surfaces. The shaded area represents the membrane and the cylinder represents the peptide. Note that $\varphi = 90°$ corresponds to a surface associated helix and that $\varphi = 180°$ and 0° correspond to N-terminal and C-terminal inserted orientations, respectively.

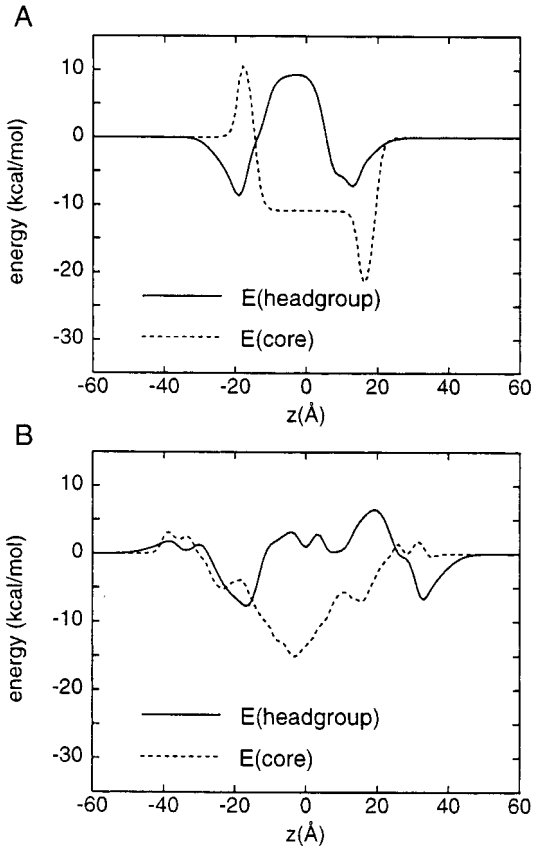

Fig. 5. Peptide–bilayer interaction energies for dermaseptin B as a function of translation relative to the bilayer. (A) Translation with the helix in a $\varphi = 90°$ orientation. (B) Translation with the helix in a $\varphi = 180°$ orientation. In both cases the solid line corresponds to $E_{\mathrm{HEADGROUP}}$ and the broken line to E_{CORE}.

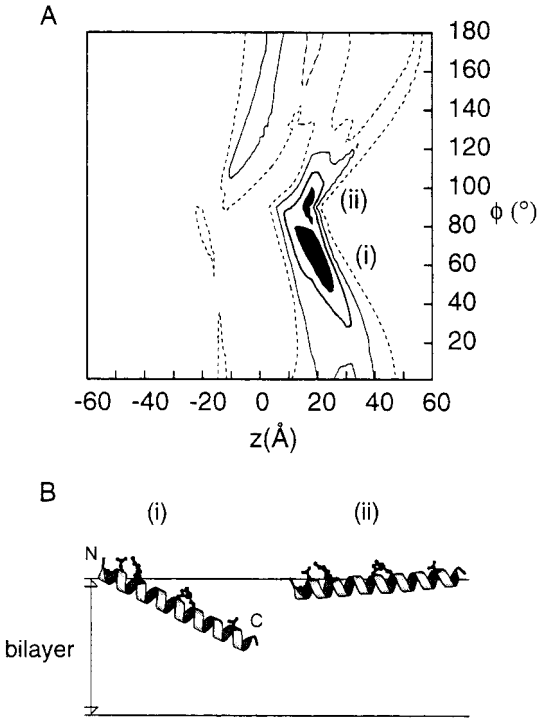

Fig. 6. (A) Peptide–bilayer energy surface for dermaseptin B shown as an equipotential contour plot. The two filled regions (i) and (ii), enclose the two energy minima (< -23 kcal/mol). The contours correspond to interaction energies of -17 (bold line), -11 (thin line), and -5 (broken line) kcal/mol. (B) Molscript (Kraulis, 1991) diagram of the orientation of the dermaseptin B helix corresponding to the two energy minima in (A). The two horizontal solid lines indicate the extent on z of the bilayer.

In order to define more exactly the minimum energy orientation(s) of DS-B relative to the lipid bilayer, the helix rotations illustrated in Fig. 4B were performed for different values of z for the centre of the helix. For each value of z, φ was varied whilst maintaining $\theta = 0°$. The results may be presented as a contour map of the $E(z,\varphi)$ surface (Fig. 6A). From this map two minima are evident, both corresponding to a 'surface bound' orientation of the peptide helix. Minimum (i) (see Fig. 6) corresponds to the DS-B helix being approximately perpendicular to the bilayer normal (ϕ approx. $-70°$) and has a value of approximately -29 kcal/mol. Minimum (ii) also corresponds to the DS-B helix in a 'surface bound' orientation, and is almost as deep (approx. -26 kcal/mol) as (i). The lower energy of minimum (i) derives mainly from interaction of certain charged residues (His16, Lys19 and Asp27 in particular) with the dipole potential. Of course, one should take care not to over interpret these results as besides other approximations the DS-B helix is treated as a rigid body, which is clearly a substantial approximation. To examine the consequences of intramolecular flexibility MD simulations were performed.

3.3. MD simulations

The interaction of a DS-B helix with a bilayer

Table 1
Summary of MD simulations on dermaseptin-B

Simulation	Fractional α-helicity (core region)	Fractional α-helicity (allowed region)
In vacuo	0.62	0.74
LE-HG	0.75	0.89
LEI-HG	0.56	0.96
LE-NOHG	0.60	0.87
HE-HG	0.82	0.96

All simulations other than the in vacuo simulations were in the presence of a bilayer potential. LE and HE indicate opposite orientations of the peptide helix at the membrane water interface corresponding to $\theta = 0°$ (apolar surface towards bilayer; i.e. 'low energy') and $\theta = 180°$ (polar surface towards bilayer, i.e. 'high energy'), respectively. LEI indicates the simulation starting with the C-terminus of the helix inserted, corresponding to minimum (i) in the rigid body energy mapping (see Fig. 6). HG and NOHG refer, respectively to the inclusion of $E_{\text{HEADGROUP}}$ in the bilayer potential function, and to the exclusion of $E_{\text{HEADGROUP}}$ from the function. Fractional helicities were estimated over the last 30 ps of each simulation, and were calculated using both the core α-helix region and the allowed α-helix regions of the Ramachandran plot as defined in Procheck ([37]).

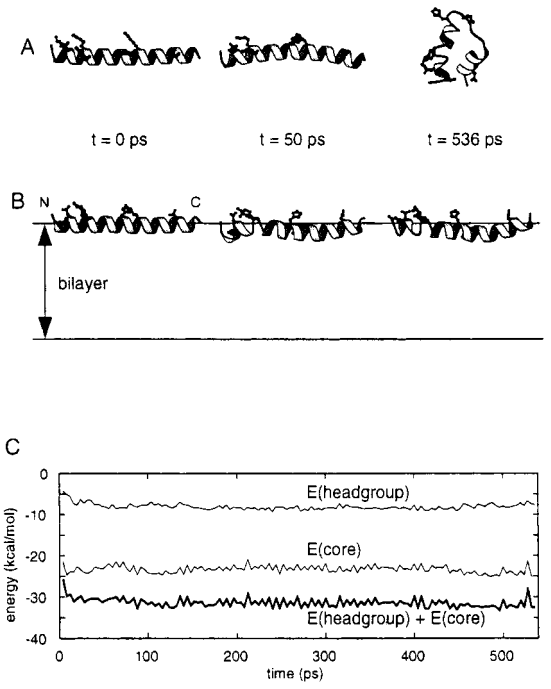

Fig. 7. (A,B) Snapshots of MD simulations of dermaseptin B at $t = 0$, 50 and 536 ps: (A) the in vacuo simulation; and (B) The LE-HG simulation. (C) Interaction energy trajectories for the LE-HG simulation.

surface whilst allowing for conformational flexibility has been explored in a series of MD simulations (see Table 1). A control in vacuo simulation was performed which did *not* include the bilayer terms [see Eq. (8)] in the potential energy function, but did use $\varepsilon = r$ for screening electrostatic interactions. Three simulations in the presence of the bilayer term were conducted. One of these (LE-HG) started with the DS-B helix at $z = +17$ Å, $\varphi = 90°$ and $\theta = 0°$, i.e. close to minimum (ii) as defined in the previous section, and had both of the bilayer energy terms included. The other two simulations were intended to test the sensitivity of the results to the bilayer energy function and to the starting orientation of the helix and are discussed below.

The most profound difference between the in vacuo and LE-HG simulation is in the conformation of the peptide. Examination of the fraction of peptide bonds falling within the α-helical regions of the Ramachandran plot for the last 30 ps of each simulation (Table 1) suggests that there is significantly less helical structure in the in vacuo simulation. However, this conceals some of the major changes in conformation of the DS-B molecule which occur during this simulation as a result of interactions between oppositely charged sidechains. The situation is more fully revealed by display of snapshots from the trajectory (Fig. 7A). From these it is evident that, although the DS-B molecule starts off as an extended α-helix, by the end of the simulation considerable loss of helicity has occurred and, furthermore, the molecule has folded back on itself to form a helical hairpin. In the presence of the bilayer potential the overall conformation of helix is considerably stabilised, although local deviations from helical geometry still occur. This is in general agreement with a number of experimental studies which suggest stabilisation of amphipathic helices by lipid bilayers, e.g. [39,40].

In order to investigate the effect of the use of a distance cutoff on long range electrostatic interactions, the LE-HG simulation was repeated but without such a cutoff, i.e. with all long distance

electrostatic interactions included. The results (not shown) were almost identical to those just discussed, suggesting that the simulations are not over-sensitive to the exact treatment of electrostatic interactions,

In terms of helix orientation the LE-HG simulation shows only a small change from the initial orientation, with the helix moving a little further into the bilayer (at $t = 0$ ps z approx. + 17 Å, at $t = 536$ ps z approx. +15.8 Å). The final orientation is close to that of minimum (ii) in the rigid body energy mapping (see above). From a number of other simulations (see below; also; [15,17]) we know that substantial helix reorientation can occur within less than approximately 100 ps. An MD simulation (LEI-HG, see Table 1) starting with an orientation corresponding to minimum (i) in the rigid body energy mapping, in which the C-terminus is partly inserted into the bilayer, was run. This resulted in a marginally less stable configuration of the system. Thus, averaging over the last 100 ps of each simulation, for LEI-HG the mean value of $(E_{\mathrm{CORE}} + E_{\mathrm{HEADGROUP}}) = -30.7\ (\pm 0.7)$ kcal/mol. The corresponding value for LE-HG (i.e. starting with DS-B parallel to the bilayer surface) is $-32.0\ (\pm 0.1)$ kcal/mol. Furthermore, there was a marked loss of helicity in the N-terminal half of DS-B during simulation LEI-HG (see Table 1). Taken in conjunction, these observations help to confirm a surface location as being most favourable for the DS-B helix.

Thus, it would seem that once internal flexibility of DS-B is taken into account a surface-associated orientation is more stable. Examination of the trajectories of the interaction energies between peptide and bilayer (Fig. 7C) show that after an initial relaxation period of less than 100 ps the total interaction energy reaches a stable value of $-32\ (\pm 1)$ kcal/mol (averaged over 200–536 ps). This is thus lower than that of either minimum in the rigid body exploration. Thus MD simulations reveal some further details of peptide–bilayer interactions.

Conservation of helicity in the LE-HG simulation may be analysed in more detail by reference to Fig. 8A. From this diagram of the time evolution of the secondary structure of DS-B it is evident that after approximately 100 ps the secondary structure reaches a steady state. There is

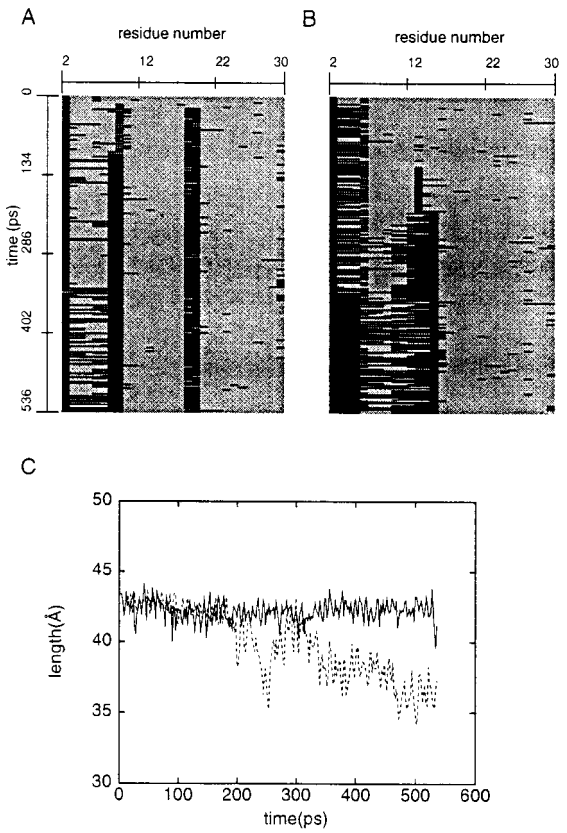

Fig. 8. Secondary structure vs. time for dermaseptin B in the (A) LE-HG and (B) LE-NOHG simulations. Grey indicates an α-helical conformation and black indicates random coil conformations. A segmental definition of α-helicity has been used whereby a residue is considered to be in an α-helical conformation only if its backbone torsion angles and those of the two neighbouring residues fall in the core α-helical region of the Ramachandran plot as defined in Procheck [37]. (C) Helix length vs. time for the LE-HS (solid line) and LE-NOHG (broken line) simulations.

loss of α-helical structure in three main regions of the molecule: N-terminus; residue Lys-8 and Lys-9; and residues Gly-18 and Lys-19. Distortion from helical geometry at the N-terminus and in the vicinity of a glycine are not surprising. The distortion at residues 8 and 9 seems to have originated from the electrostatic interaction of the lysines with Asp-5. There are also mainchain to lysine sidechain H-bonds involving these residues. However, one should not overemphasise these interactions as (aqueous) solvation was not included in anything other than a very approximate manner (i.e. $\varepsilon = r$).

In order to examine the effect of changing the nature of the bilayer interaction potential, a simulation — LE-NOHG — was performed in which the $E_{\mathrm{HEADGROUP}}$ term was omitted but the E_{CORE} term was retained. As can be seen from Table 1 and Fig. 8B this leads to considerable loss of helicity after approximately 200 ps of the simulation has elapsed, particularly in the N-terminal half of the molecule. By the end of the simulation the helicity has dropped to approximately 60%, in contrast with approximately 75% for the LE-HG simulation. Furthermore, the helix length (Fig. 8c) in LE-NOHG drops by about 5 Å whereas in LE-HG the length remains constant. Thus it seems that both hydrophobic and electrostatic interactions with the bilayer lead to stabilisation of the DS-B α-helix. The relative balance of these might be altered by a non-zero ionic strength. Comparable simulations on dermaseptin b (which corresponds to DS-B minus the first four residues) reveal a similar effect (data not shown). Thus these results are relatively robust to minor changes in the sequence of the peptide.

In these simulations it has been assumed, on the basis of rigid body calculations, that the most stable helix orientation is that in which the polar face of the helix is directed away from the bilayer interior (i.e. $\theta = 0°$). To test this, and also to see whether the DS-B helix can undergo substantial changes in orientation during approximately 500 ps of MD, a simulation (HE-HG) was performed which started with the helix oriented such that its polar sidechains were pointing into the bilayer core. The results of this simulation confirm that substantial changes in DS-B helix orientation may occur and that the same final stable orientation is reached as in the LE-HG simulation. Thus, examination of snapshots from the trajectory (Fig. 9A) shows that within the first 50 ps the helix is drawn a little deeper into the bilayer. Over the next 50 ps it then rotates so that the polar sidechains point away from the centre of the bilayer. This reorientation can be seen quite clearly if one compares the trajectories of θ for the LE-HG and HE-HG simulations (Fig. 9B) from which it is evident that in the latter case the helix reorients during the first 100 ps and then stays in the same orientation as in the LE-HG simulation. The interaction energy trajectory for

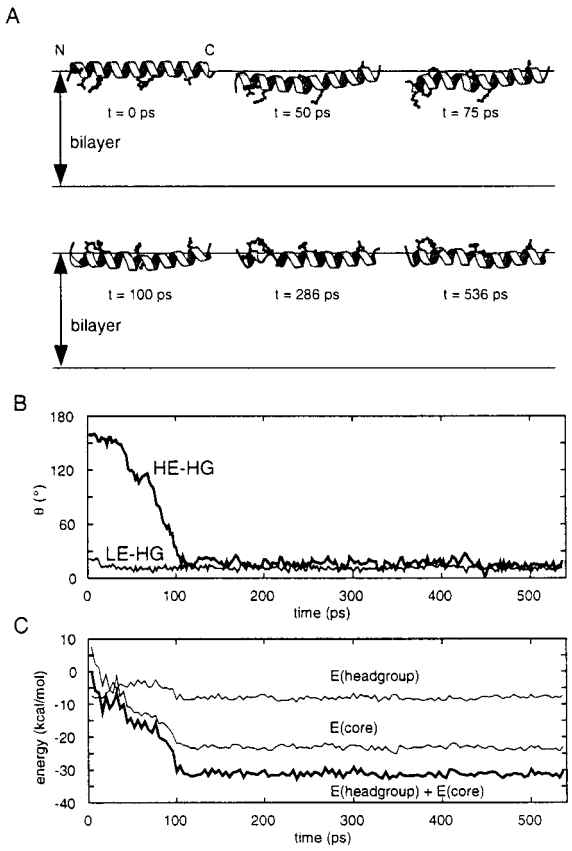

Fig. 9. (A) Snapshots of the HE-HG simulation for dermaseptin B at $t = 0$, 50, 75, 100, 268, and 536 ps. (B) Trajectories of θ (see Fig. 4A) for the LE-HG and HE-HG simulations. (C) Energy trajectories for the HE-HG simulation.

the HE-HG simulation falls during the first 100 ps as the helix reorients itself. From then onwards the HE-HG and LE-HG simulations yield essentially the same results. The fractional helicity over the last 100 ps of the simulation is independent of the starting orientation (see Table 1). It is interesting to note that such a rotation of amphipathic helices bound to a bilayer surface was discussed in an earlier model of peptide–bilayer interactions [41].

4. Discussion

4.1. Methodology

There are a number of assumptions implicit in our simulation methodology which merit discus-

sion. The first involves use of a fixed membrane force field, which does not change upon peptide insertion. In this respect our calculation might be regarded as the first step of a hypothetical iterative procedure at each step of which one examines the effects of one of the two interacting elements (peptide and bilayer) on the other, keeping the latter fixed in the output configuration of the previous step. As a first approximation we have examined the effects on peptide orientation and conformation in the membrane of an *unperturbed* lipid bilayer. The bilayer is assumed to have two main effects. It creates an anisotropic environment for the peptide, which is hydrophobic in the core of the membrane. It also gives rise to electrostatic fields at the bilayer–water interface generated by charges on the headgroups of the lipids.

First consider the effects of the hydrophobic bilayer environment. As a peptide moves from the aqueous phase to the bilayer interior it will 'desolvate'. Associated with this process are the various entropic and enthalpic contributions to the free energy of transfer of the peptide from the aqueous phase to the hydrophobic core of the membrane which constitute the hydrophobic effect. In our procedure we assign a hydrophobicity value to each amino acid, which takes account of this effect. Furthermore desolvation effects the strength of the intramolecular electrostatic interactions. In our method we use a uniform distance-dependent dielectric constant for the screening of such interactions, which is clearly a substantial approximation. We have shown that the simulation results are not unduly sensitive to the treatment of electrostatic interactions by repeating the simulation with and without a long distance cutoff. If one attempted to screen intramolecular interactions using a z-dependent dielectric constant electrostatic interactions between charged side chains within the bilayer interior would be stronger than in the aqueous phase. However, as an ionisable sidechain moves into the bilayer core, it is likely to loose or gain a proton in order to become electrically neutral. This might be expected to counteract the decrease in dielectric constant on entering the bilayer. So, it is probably safer not to alter the treatment of the dielectric without simultaneously allowing for dynamic changes in the charge state of ionisable residues. Thus our approach is likely to provide a reasonable first approximation to the true situation. A more accurate treatment *might* be possible via MD simulations including an explicit bilayer [24] and which *also* allowed dynamic changes in the protonation state of ionisable groups during the course of the simulation. This is a difficult problem which will require the development of force fields (e.g. PM6 for water [42,43] which allow for dynamic protonation/deprotonation of peptides (and of lipid).

Another effect of the presence of the lipid bilayer is to create high electrostatic fields at the bilayer-water interface. In discussions of the electric potential profile through a membrane several authors [26,44] consider separate components, namely: a transbilayer potential (arising from the distribution of ions across a cell membrane and the resting membrane permeability to K^+ ions [45]; a surface potential, arising from the net surface charge of the membrane; and a 'dipole' potential arising from the molecular dipoles (of the phospholipid headgroup, glycerol and ester groups, and ordered water molecules) in the 'interfacial' region. In our simulations we have considered a bilayer composed of zwitterionic phospholipids, without a net electrostatic potential (i.e. voltage) difference between the two sides of the bilayer. Thus the electrostatic potential is made up only of the 'dipolar' term. This has been derived from the distribution of partial atomic charges taken from a single published MD simulation of a PC bilayer [19]. However, in principle such a one dimensional distribution of charge could be derived from other MD simulations of bilayers [20–24] or from experimental (X-ray and neutron diffraction) studies of the distribution of bilayer components along the bilayer normal [18]. Thus the method is of general applicability. Its main limitation lies in the way in which water has been treated. Several authors have stressed the possible contribution of water dipoles at the interface to the positive potential in the centre of a membrane [21,31,32,46].

In our calculation the effect of water molecules is approximated by a non-uniform dielectric con-

stant characterised in terms of the two parameters z and h. Although the choice of z and h to give a reasonable value of the 'dipole potential' is not unique, the resulting potential is fairly stable, in its general features, with respect to variations in d and h. For example the position of the potential well is independent of d and h. Discussions of the results of MD simulations of pure lipid bilayers in the absence of peptides have tended to stress the overcompensation by water dipoles of an otherwise negative potential due to the lipid head-groups. In trying to relate the results of such calculations with experiments on the differential permeability of hydrophobic ions (as used to measure the 'dipole' potential) one should bare in mind that a bulky hydrophobic ion is likely to perturb the local ordering of water. Indeed, any bulky molecule at the interface, e.g. a hydrophobic ion or a peptide, will change the relative importance of the water and lipid head-group contributions to the electrostatic potential of the pure lipid bilayer, possibly in favour of the latter. Therefore a first approximation to the dipole potential that treats the interfacial water in a simple fashion may be more appropriate to peptide–bilayer simulations.

It is not clear in the context of peptide–bilayer simulations whether using an overall (i.e. explicit bilayer dipole plus explicit water dipoles) dipole potential would be a better approximation than the simplification used in the current study. There are a number of factors that need to be taken into consideration. Firstly, dipole potentials calculated from the difference between the lipid head-group dipoles and the compensating water dipoles in explicit water plus bilayer simulations [21,23] arise from a relatively small difference between two large opposing terms. Therefore they may be expected to be somewhat sensitive to the exact parameterisation of lipid and water. Furthermore, the presence of a peptide at the bilayer–water interface will displace (some of) the water and so the peptide may experience a different potential from that calculated as the difference between the water and dipole potentials in a pure bilayer simulation. In the light of these considerable theoretical difficulties, we feel that the simple approach adopted here is a reasonable first approximation. Indeed, it is likely that the simulation results using the method described in the current paper are relatively robust to changes in the shape of the $E_{\mathrm{HEADGROUP}}$ term, provided that the overall sign and magnitude of the difference in potential between the bilayer interior and interfacial region is modelled correctly.

The peptide is modelled at the start of the simulations as an α-helix. Consistently we used a hydrophobicity scale for residues in their helical conformation. For the sake of simplicity we retained the same hydrophobicity scale throughout the simulation even though some of the residues loose helicity. This approximation does not detract from our conclusions, as we are mainly interested in the stability of the α-helical conformation of the peptide. Thus, if the peptide shows a high tendency to remain in an α-helical conformation, the hydrophobicity scale used is appropriate. The analysis of peptide conformation (e.g. Fig. 8A) shows that for most residues an α-helical conformation is retained for most of the time. As mentioned above in the context of intramolecular electrostatic interactions we treat the ionizable residues as having a fixed protonation state. This approximation is also likely to lead to an overestimation of the magnitude of the electrostatic interaction with the membrane. We are currently investigating an approximate correction for this effect by an empirical 'scaling down' of the charges of titratable residues as they penetrate the bilayer core. Preliminary results (La Rocca and Sansom, unpublished data) suggest that such a correction may alter the relative stability of the two minima in Fig. 6 in favour of minimum (ii).

Despite the approximations implicit in our calculations, we remain confident in the main conclusion, i.e. that the bilayer–water interface stabilises the α-helical conformation of DS-B. It should be noted that preliminary results employing the current methodology for alamethicin indicate a strong propensity of this peptide to insert into a bilayer, in agreement with earlier simulations [17] and with experimental data (reviewed by [11]). This validates our methodology as in this example our method seems to be able to distinguish between a preferred interfacial vs. inserted location for a peptide.

4.2. Biological implications

The most important result that emerges from this study is that DS-B preferentially interacts with the surface of a PC bilayer, rather than inserting into the bilayer to span it, and that this interaction significantly stabilizes the secondary structure of DS-B. Such stabilisation of secondary structure by bilayer interactions has been suggested a number of times for amphipathic helical peptides, both experimentally and theoretically [13,39,47–49]. An α-helical conformation for DS-B in a bilayer environment is supported by the FTIR data reported in this paper, whereas the same peptide is seen to be disordered when in aqueous solution. A surface location, rather than an inserted location, for DS-B is supported by the interfacial location of the N-terminus of the peptide as detected by fluorescence [9] and by the observation that similar dermaseptin peptides bound to PC vesicles remains susceptible to proteolytic digestion [50]. A surface location has been proposed for the related amphibian anti-microbial peptide, magainin, on the basis of solid state NMR measurements [51] and was also supported by (somewhat more simplified) simulation studies [13]. FTIR-ATR measurements and simulation studies also support a surface location for cecropin P1, a mammalian anti-microbial peptide [10]. Thus it seems likely that DS-B may act, as do several other peptides, via a 'carpet' mechanism [2] whereby the primary interaction of the peptide helix is with the surface of the membrane. However, the nature of the subsequent membrane destabilisation events, which may require peptide–peptide interactions at the membrane surface, has yet to be addressed via simulations.

Overall, the simulation approach adopted in this paper appears to give reasonable correlation with experimental observations and provide a molecular description of the early stages of interactions of an anti-microbial peptide may interact with a lipid bilayer. It should be noted that these simulations do not address the possibility of peptide–peptide interactions which might conceivably facilitate peptide insertion into a bilayer. However, the correlation between experiments and simulations suggest that computational studies may prove to be a valuable tool in the design of novel anti-microbial peptides with improved selectivity and biological activity. The methods described in this paper are currently being extended to other peptides (e.g. caerins; Wong et al. [52]) and toxins (e.g. δ-endotoxin; [41,53]), and is being extended to negatively charged phospholipids, such as PS for which MD simulated structures are now available [22]. It will be interesting to compare the results of our simulations for PS bilayers with the studies of McLaughlin et al. [54–56] who have used electrostatic calculations to explore the interactions of basic peptides and proteins with a model PC:PS bilayer. It will also be interesting to compare results of simulations using a continuum approximation to peptide–bilayer interactions with those simulations in which the lipid bilayer and water are treated atomistically, as in a recent simulation study of melittin [57]. Encouragingly, preliminary simulations of DS-B at the surface of a fully solvated phospholipid bilayer (La Rocca and Sansom, manuscript in preparation) yield results which support those obtained in the current study.

Acknowledgements

This work was supported by a grants from the UK-Israel Science and Technology Research Fund, the Wellcome Trust, and the BBSRC. Our thanks to Dr I.D. Kerr and P.C. Biggin for their interest in this work.

References

[1] H.G. Boman, Ann. Rev. Immunol. 13 (1995) 61–92.
[2] Y. Shai, Trends. Biochem. Sci. 20 (1995) 460–464.
[3] M.S.P. Sansom, Prog. Biophys. Mol. Biol. 55 (1991) 139–236.
[4] A. Mor, V.H. Nguyen, A. Delfour, D. Migliore-Samour, P. Nicolas, Biochemistry 30 (1991) 8824–8830.
[5] M. Amiche, F. Ducancel, A. Mor, J.C. Boulain, A. Menez, P. Nicolas, J. Biol. Chem. 269 (1994) 17847–17852.
[6] A. Mor, K. Hani, P. Nicolas, J. Biol. Chem. 269 (1994) 31635–31641.
[7] A. Mor, M. Amiche, P. Nicolas, Biochemistry 33 (1994) 6642–6650.
[8] A. Mor, P. Nicolas, Eur. J. Biochem. 219 (1994) 145–154.

[9] J. Strahilevitch, A. Mor, P. Nicolas, Y. Shai, Biochemistry 33 (1994) 10951–10960.
[10] E. Gazit, I.R. Miller, P.C. Biggin, M.S.P. Sansom, Y. Shai, J. Mol. Biol. 258 (1996) 860–870.
[11] M.S.P. Sansom, Quart. Rev. Biophys. 26 (1993) 365–421.
[12] O. Edholm, F. Jähnig, Biophys. Chem. 30 (1988) 279–292.
[13] M. Milik, J. Skolnick, Proteins: Struct. Func. Genet. 15 (1993) 10–25.
[14] N. Ben-Tal, A. Ben-Shaul, A. Nicholls, B. Honig, Biophys. J. 70 (1996) 1803–1812.
[15] P.C. Biggin, M.S.P. Sansom, Biophys. Chem. 60 (1996) 99–110.
[16] P. Ducarme, N. Rahman, R. Brasseur, Proteins Struct. Funct. Genet. 30 (1998) 357–371.
[17] P.C. Biggin, J. Breed, H.S. Son, M.S.P. Sansom, Biophys. J. 72 (1997) 627–636.
[18] M.C. Wiener, S.H. White, Biophys. J. 61 (1992) 428–433.
[19] H. Heller, M. Shaefer, K. Shulten, J. Phys. Chem. 97 (1993) 8343–8360.
[20] A.J. Robinson, W.G. Richards, P.J. Thomas, M.M. Hann, Biophys. J. 67 (1994) 2345–2354.
[21] S.-W. Chiu, M. Clark, V. Balaji, S. Subramaniam, H.L. Scott, E. Jakobsson, Biophys. J. 69 (1995) 1230–1245.
[22] J.J.L. Cascales, J.G. de la Torre, S.J. Marrink, H.J.C. Berendsen, J. Chem. Phys. 104 (1996) 2713–2720.
[23] D.P. Tieleman, H.J.C. Berendsen, J. Chem. Phys. 105 (1996) 4871–4880.
[24] D.P. Tieleman, S.J. Marrink, H.J.C. Berendsen, Biochim. Biophys. Acta 1331 (1997) 235–270.
[25] R.F. Flewelling, W.L. Hubbel, Biophys. J. 49 (1986) 541–552.
[26] D.S. Cafiso, Curr. Opin. Struct. Biol. 1 (1991) 185–190.
[27] B.R. Brooks, R.E. Bruccoleri, B.D. Olafson, D.J. States, S. Swaminathan, M. Karplus, J. Comp. Chem. 4 (1983) 187–217.
[28] P. La Rocca, M.S.P. Sansom, Y. Shai, A. Mor, Protein Sci. 6 (1997) 54.
[29] W.H. Press, S.A. Teukolsky, W.T. Vetterling, B.P. Flannery, Numerical Recipes in FORTRAN — The Art of Scientific Computing, Cambridge University Press, 1992.
[30] O.H.J. LeBlanc, Biophys. J. (Abstr.). 14 (1970) 94a.
[31] S.A. Simon, T.J. McIntosh, Proc. Natl. Acad. Sci. USA 86 (1989) 9263–9267.
[32] K. Gawrisch, D. Ruston, J. Zimmerberg, V.A. Parsegian, R.P. Rand, N. Fuller, Biophys. J. 61 (1992) 1213–1223.
[33] O. Edholm, F. Jähnig, Biophys. Chem. 30 (1988) 279–292.
[34] I.D. Kerr, R. Sankararamakrishnan, O.S. Smart, M.S.P. Sansom, Biophys. J. 67 (1994) 1501–1515.
[35] A.T. Brünger, X-PLOR Version 3.1. A System for X-ray Crystallography and NMR., Yale University Press, CT., 1992.
[36] P.J. Kraulis, J. Appl. Cryst. 24 (1991) 946–950.
[37] A.L. Morris, M.W. MacArthur, E.G. Hutchinson, J.M. Thornton, Proteins Struct. Funct. and Genet. 12 (1992) 345–364.
[38] M. Jackson, H.H. Mantsch, Crit. Rev. Biochem. Mol. Biol. 30 (1995) 95–120.
[39] E.T. Kaiser, F.J. Kezdy, Proc. Natl. Acad. Sci. USA 80 (1983) 1137–1143.
[40] W.F. DeGrado, Z.R. Wasserman, J.D. Lear, Science 243 (1989) 622–628.
[41] E. Gazit, Y. Shai, J. Biol. Chem. 270 (1995) 2571–2578.
[42] F.H. Stillinger, C.W. David, J. Chem. Phys. 71 (1978) 1647–1651.
[43] T.A. Weber, F.H. Stillinger, J. Phys. Chem. 86 (1982) 1314–1318.
[44] B.H. Honig, W.L. Hubbell, R.F. Flewelling, Ann. Rev. Biophys. Chem. 15 (1986) 163–193.
[45] B. Hille, Ionic Channels of Excitable Membranes, 2nd ed., Sinauer Associates, Sunderland, Mass., 1992.
[46] C. Zheng, G. Vanderkooi, Biophys. J. 63 (1992) 935–941.
[47] M.R. Wattenbarger, H.S. Chan, D.F. Evans, V.A. Bloomfield, K.A. Dill, J. Chem. Phys. 93 (1990) 8343–8351.
[48] H.S. Chan, M.R. Wattenbarger, D.F. Evans, V.A. Bloomfield, K.A. Dill, J. Chem. Phys. 94 (1991) 8543–8557.
[49] M. Milik, A. Kolinski, J. Skolnick, J. Phys. Chem. 96 (1992) 4015–4022.
[50] Y. Pouny, D. Rapaport, A. Mor, P. Nicolas, Y. Shai, Biochemistry 31 (1992) 12416–12423.
[51] B. Bechinger, M. Zasloff, S.J. Opella, Protein Sci. 2 (1993) 2077–2084.
[52] H. Wong, J.H. Bowie, J.A. Carver, Eur. J. Biochem. 247 (1997) 545–557.
[53] E. Gazit, D. Bach, I.D. Kerr, M.S.P. Sansom, N. Chejanovsky, Y. Shai, Biochem. J. 304 (1994) 895–902.
[54] S.L. Carnie, G.M. Torrie, in: S.A. Rice (Eds.), Advances in Chemical Physics I. Prigogine, John Wiley, New York, USA, 1984, pp. 141–253.
[55] N. Ben-Tal, B. Honig, R.M. Peitzsch, G. Denisov, S. McLaughlin, Biophys. J. 71 (1996) 561–575.
[56] D. Murray, N. Ben-Tal, B. Honig, S. McLaughlin, Structure 5 (1997) 985–989.
[57] S. Bernèche, M. Nina, B. Roux, Biophys. J. 75 (1998) 1603–1618.